AIP | Journal of Applied Physics

Dimensional considerations in achieving large quality factors for resonant silicon cantilevers in air

Kianoush Naeli and Oliver Brand

Citation: J. Appl. Phys. **105**, 014908 (2009); doi: 10.1063/1.3062204
View online: http://dx.doi.org/10.1063/1.3062204
View Table of Contents: http://jap.aip.org/resource/1/JAPIAU/v105/i1
Published by the American Institute of Physics.

Dimensional considerations in achieving large quality factors for resonant silicon cantilevers in air

Kianoush Naeli[a] and Oliver Brand
School of Electrical and Computer Engineering, Georgia Institute of Technology, Atlanta, Georgia 30332, USA

(Received 21 September 2008; accepted 21 November 2008; published online 13 January 2009)

This work aims to provide guidelines for designing rectangular silicon cantilever beams to achieve maximum quality factors for the fundamental flexural resonance at atmospheric pressure. The methodology of this work is based on experimental data acquisition of resonance characteristics of silicon cantilevers, combined with modification of analytical damping models to match the captured data. For this purpose, rectangular silicon cantilever beams with thicknesses of 5, 7, 8, 11, and 17 μm and lengths and widths ranging from 70 to 1050 μm and 80 to 230 μm, respectively, have been fabricated and tested. Combining the three dominant damping mechanisms, i.e., the air damping, support loss, and thermoelastic damping, the variation in the measured Q-factors with the cantilever geometrical dimensions is predicted. Also to better describe the experimental data, modified models for air damping have been developed. These modified models can predict the optimum length and thickness of a resonant cantilever to achieve the maximum quality factor at the fundamental flexural resonance mode in air. © *2009 American Institute of Physics*.
[DOI: 10.1063/1.3062204]

I. INTRODUCTION

Resonant cantilever sensors have been used in a variety of chemical and biochemical sensing applications.[1–5] The operation principle in most of these sensors is based on detection of a resonance frequency shift as a result of interaction with the targeted subject.[6–8] An important parameter for this detection scheme is the quality factor (Q or Q-factor) of the resonator: a larger quality factor results in better frequency stability and consequently better sensing resolution.[9,10] Also, in force detection techniques with cantilevers, e.g., in atomic force microscopy and magnetic resonance force microscopy, the thermomechanical noise of cantilever sensors is reduced by increasing the Q-factor.[11–13]

For a simple resonator, higher Q-factors can be obtained either by improving the quality of the resonator structural material[14] or by optimizing the resonator shape to decrease the energy loss of the system. For a simple microcantilever beam resonating in air, since the choice of material is usually limited to what is commonly provided in microfabrication technology, e.g., silicon, silicon nitride, and silicon oxide, the effect of cantilever's geometrical dimensions on the Q-factor becomes an attractive subject to study. In this regard, the focus of this paper is on the fundamental flexural resonance mode of rectangular silicon cantilever beams resonating in air. The goal of this paper is to find the optimum dimensions for such cantilevers to achieve maximum Q-factors.

The quality factor is a measure of energy loss in a system. As long as the stored energy is constant, the higher quality factor means the lower energy dissipation per cycle. The quality factor of a cantilever resonating in air can be attributed to two main loss mechanisms: extrinsic and intrinsic. The extrinsic loss is due to interactions with the surrounding medium, e.g., viscous losses[15–17] and acoustic radiation.[18,19] The intrinsic loss is due to interactions within the cantilever structure or with its support structure, e.g., support loss,[20] thermoelastic loss [thermoelastic damping (TED)],[21–23] volume loss,[17,24] and surface loss.[24–26] The total energy dissipation in a system is calculated by adding the energy dissipation of each individual loss mechanism. Hence, for a given resonance frequency, the quality factor of the system is obtained from the quality factors attributed to each individual loss mechanism Q_{indiv},

$$\frac{1}{Q} = \sum \frac{1}{Q_{\text{indiv}}} = \frac{1}{Q_{\text{air}}} + \frac{1}{Q_{\text{clamp}}} + \frac{1}{Q_{\text{TED}}} + \frac{1}{Q_{\text{vol}}} + \frac{1}{Q_{\text{surf}}}. \tag{1}$$

The individual Q-factors Q_{indiv} are calculated as if there is no other loss mechanism except the investigated one, e.g., air, support (clamp), thermoelastic, volume, or surface loss. For cantilevers resonating at atmospheric pressure, the dominant damping mechanism is the viscous (air) damping;[15,25] on the other hand, in vacuum, where the resonators generally have significantly larger Q-factors, the support loss becomes more dominant when decreasing the cantilevers length.[25–27] In this section, the three main damping mechanisms for a resonant cantilever, the air damping, support loss, and TED, are reviewed.

A. Air (viscous) damping

To analytically describe the air damping of a transversely resonating cantilever, three major approaches are proposed in the literature.[28–30] All these approaches rely on analytically well-known solutions for the viscous damping of

[a]Electronic mail: kianoush@gatech.edu. Tel.: +1-404-894-9917. FAX: +1-404-894-4700.

basic solid bodies, which are derived from the Navier–Stokes equation and the continuity equation for incompressible fluids,[31]

$$\frac{\partial \mathbf{u}}{\partial t} + (\mathbf{u} \cdot \nabla)\mathbf{u} = -\frac{1}{\rho_o} \nabla P + \frac{\eta}{\rho_o} \Delta \mathbf{u}, \tag{2}$$

$$\nabla \cdot \mathbf{u} = 0, \tag{3}$$

where $\mathbf{u}(x,y,z,t)$ is the velocity field of the medium, P is the medium pressure, η and ρ_o are the dynamic viscosity and the density of the medium, respectively.

In the first analytical approach, the air damping of the cantilever is approximated by the viscous damping of a plate that undergoes a steady motion in the normal direction to the surface.[28,32] In the second approach the beam is visualized as a single or a string of coherently resonating spheres, and based on the damping of each sphere, the total damping is calculated.[15,29,33–37] In the last approach, the beam vibration is described based on the vibration of a cylinder in a viscous medium.[30,38,39] In most of the models derived based on these approaches, a general assumption is to have a flow with a small Reynolds number. The Reynolds number R_e for a resonating beam is defined as[30]

$$R_e = \frac{\rho_o \omega}{4\eta} W^2, \tag{4}$$

where W is the width of the beam and ω is the angular resonance velocity. The requirement for a small Reynolds number implies that there are possibly less accurate predictions for higher resonance frequencies or for wider cantilevers.

In describing the air damping, the first analytical approach only accounts for the continuous movement of the cantilever through the medium (steady flow), while this model neglects the presence of resonant flows. This shortcoming is addressed in the other two approaches. In the second approach, i.e., the string of spheres model, the streamline around the cantilever beam can be considered the same as a streamline around a sphere when the Reynolds number is fairly small ($R_e < 1$).[15,35] An analytical expression for the oscillatory motion of a sphere in a viscous fluid has been derived by Landau and Lifshitz[31] based on which Blom *et al.*[15] calculated the Q-factor of an oscillating beam in a viscous medium. In Blom's model, the whole cantilever beam is approximated with a single sphere, whose radius is obtained by curve fitting the experimental results. Hosaka *et al.*[35] expanded the analytical expression of this model by considering the entire cantilever structure as a string of identical spheres. The diameter of each sphere is equal to the width of the beam. According to this model, the quality factor associated with the air damping Q_{air} is calculated as

$$Q_{\text{air}} = \frac{\rho_b H W^2 \omega_n}{3\pi\eta W + \frac{3}{4}\pi W^2 \sqrt{2\rho_a \eta \omega_n}}, \tag{5}$$

where ρ_b and ρ_a are the densities of the beam and air, respectively, H is the thickness of the beam, and ω_n is the angular velocity of the nth flexural mode. This model, however, does not include the effect of the drag force on the areas of the beam that the spheres do not cover. This issue is addressed by empirically calculating an effective sphere radius based on the measurement data.[36,40]

The third approach, applying the vibration solution of a resonating cylinder instead of a string of spheres, can alleviate the issue of incomplete coverage of spheres over the beam structure. The analytical solution of the Navier–Stokes equation for oscillation of a cylinder in a viscous medium is well known.[39,41] Sader[30] and Kirstein *et al.*[39] approximated the damping of a resonating cantilever with that of an infinitely long cylinder. In Sader's model, the assumptions are that the length of the beam L greatly exceeds the width W, and also the width greatly exceeds the beam thickness H. The accuracy of this model is improved by using a complex frequency dependent correction factor.[30]

B. Support loss

For a cantilever with an infinite width [a two-dimensional (2D) assumption] and with the cantilever support considered as a semi-infinite large elastic body, the damping due to elastic energy radiation to the support from the cantilever is proportional to the cube of thickness to length ratio[27] $(H/L)^3$. Hence, the quality factor Q_{clamp} of a resonator enduring only the support loss is estimated as

$$Q_{\text{clamp}} = \kappa \left(\frac{L}{H}\right)^3, \tag{6}$$

where κ is a coefficient calculated as $\kappa = 0.34$,[5] 2.17,[26,35] or 2.081.[27] In practice, the support usually does not have the exact shape assumed in the 2D theoretical derivations. In a special case, when the support is a plate as thin as the cantilever beam,[20,42] the deteriorated quality factor is proportional to L/H.

C. Thermoelastic damping

In the absence of the air damping and support loss, one of the most influential loss mechanism is the TED.[22,26] The basic analytical calculations for TED in resonant structures, especially beams in flexural mode, are derived by Zener.[21] In Zener's model the thermoelastic quality factor Q_{TED} of an isotropic homogenous beam resonating in the fundamental flexural mode is approximated by

$$Q_{\text{TED}} = \frac{\rho_b C_p}{E\alpha^2 T_o} \frac{1 + (\omega_1 \tau_Z)^2}{\omega_1 \tau_Z}, \tag{7}$$

with

$$\tau_Z = \frac{\rho_b C_p H^2}{\pi^2 \kappa_{\text{th}}},$$

where C_p is the specific heat capacity, E is the beam modulus of elasticity, α is the linear thermal expansion coefficient, T_o is the equilibrium temperature, and κ_{th} is the thermal conductivity. Although Zener's model provides a good estimate of Q_{TED} for a resonating cantilever beam at the fundamental flexural mode, a better accuracy especially for more complicated structures, e.g., laminated beams, requires a more complex modeling.[43]

TABLE I. Material properties of silicon and air.

	Quantity	Symbol	Value
Air (T_o=27 °C)	Density[a] (kg m^{-3})	ρ_a	1.18
	Dynamic viscosity[a] (Pa s)	η	18.6×10^{-6}
Silicon	Density[b] (kg m^{-3})	ρ_b	2330
	Specific heat capacity[c] (J kg^{-1} K^{-1})	C_p	700
	Modulus of elasticity[b] ⟨110⟩ (GPa)	E	169
	Linear thermal expansion coefficient[c] (K^{-1})	α	2.6×10^{-6}
	Thermal conductivity[b] (W m^{-1} K^{-1})	κ_{th}	156

[a]Reference 16.
[b]Reference 46.
[c]Reference 26.

In the presented work, in continuation of our previous work,[44] the goal is to optimize the cantilever dimensions in order to maximize the Q-factor of the fundamental flexural resonance mode in air and establish design guidelines for cantilever-based resonators. To this end, the relationships between the Q-factor and the cantilever length, width, and thickness are studied by measuring the transfer characteristic of various rectangular silicon cantilever resonators and by comparing the experimental data to analytical derivation. As an eminent result, accurate models for air damping are extracted.

II. THEORY

In this work, despite the mathematical elegance of Sader's model, we have chosen to use the more physically comprehensible approach of the string of spheres as a backbone for modeling the Q-factor of resonating cantilevers. It can be seen from Eq. (5) that the Q-factor is almost independent of the beam width if

$$\tfrac{3}{4}\pi W^2\sqrt{2\rho_a\eta\omega_n} \gg 3\pi\eta W,$$

which defines the following requirement for the resonance frequency of the beam:

$$f_n \gg \frac{1}{2\pi}\frac{8\eta}{\rho_a W^2}. \tag{8}$$

Therefore, for microcantilever beams with a width of larger than 100 μm, to satisfy the condition of Eq. (8) at the room temperature (see Table I), the required resonance frequency should be larger than 20 kHz, i.e., typically at least ten times larger than the right side of Eq. (8). The flexural resonance frequency of a cantilever beam is given by[45]

$$f_n = \frac{\omega_n}{2\pi} = \frac{\lambda_n^2}{2\pi\sqrt{12}}\frac{H}{L^2}\sqrt{\frac{E}{\rho_b}}, \tag{9}$$

where λ_n is the flexural mode identifier constant with λ_1 =1.875. By placing Eq. (9) in Eq. (5), provided that the condition of Eq. (8) is satisfied, a simplified expression for Q_{air} is obtained,

$$Q_{\text{air}} = \frac{2}{3}\frac{\lambda_n}{\pi}\left(\frac{\rho_b^3 E}{3\rho_a^2\eta^2}\right)^{1/4}\frac{\sqrt{H^3}}{L}. \tag{10}$$

Equation (10) is a function of the cantilever geometry through the ratio χ defined as

$$\chi = \frac{L}{\sqrt{H^3}}, \tag{11}$$

and also is a function of the material properties of the beam as well as the ambient conditions through the coefficient ε,

$$\varepsilon = \frac{3}{2}\frac{\pi}{\lambda_n}\left(\frac{3\rho_a^2\eta^2}{\rho_b^3 E}\right)^{1/4}. \tag{12}$$

Hence, Q_{air} can be simply described by a reciprocal relationship with χ,

$$\frac{1}{Q_{\text{air}}} = \varepsilon\chi. \tag{13}$$

Revisiting Eq. (6), Q_{clamp} can also be expressed as a function of χ,

$$Q_{\text{clamp}} = \kappa H^{3/2}\chi^3. \tag{14}$$

Using Eqs. (1), (13), and (14), the combined quality factor Q can be calculated as

$$\frac{1}{Q} = \frac{1}{Q_{\text{clamp}}} + \frac{1}{Q_{\text{air}}} = \varepsilon\chi + \kappa^{-1}H^{-3/2}\chi^{-3}. \tag{15}$$

The maximum Q is found at the optimum χ_{opt},

$$\chi_{\text{opt}} = \frac{1}{\sqrt[4]{\frac{\varepsilon\kappa}{3}H^{3/2}}}. \tag{16}$$

In other words, for a simplified case that the loss mechanism is dominated by only the air damping and support loss, the maximum Q-factor is obtained when the beam length and thickness fulfill the ratio

$$\frac{L}{H^{9/8}} = \sqrt[4]{\frac{3}{\varepsilon\kappa}}. \tag{17}$$

The accuracy of this calculation can be improved by including the effect of TED. For a simple rectangular beam resonating at the fundamental flexural mode, Q_{TED} is approxi-

mated by Eq. (7), which can be rearranged with respect to χ after applying Eq. (9),

$$Q_{\mathrm{TED}} = \frac{\rho_b C_p}{E\alpha^2 T_o} \frac{1+(\beta\chi^{-2})^2}{\beta\chi^{-2}}, \tag{18}$$

where β is

$$\beta = \frac{\rho_b C_p}{\kappa_{\mathrm{th}}} \left(\frac{\lambda_1}{\pi}\right)^2 \sqrt{\frac{E}{12\rho}}. \tag{19}$$

Using Eqs. (1), (13), (14), and (18), the combined quality factor Q can be written as

$$\frac{1}{Q} = \frac{1}{Q_{\mathrm{clamp}}} + \frac{1}{Q_{\mathrm{air}}} + \frac{1}{Q_{\mathrm{TED}}} = \varepsilon\chi + \kappa^{-1}H^{-3/2}\chi^{-3} + \frac{E\alpha^2 T_o}{\rho_b C_p} \frac{\beta\chi^{-2}}{1+(\beta\chi^{-2})^2}. \tag{20}$$

Hence for the independent variable χ, the maximum Q occurs when

$$\varepsilon - 3\kappa^{-1}H^{-3/2}\chi^{-4} - \frac{2E\alpha^2 T_o \beta}{\rho_b C_p} \frac{1-(\beta\chi^{-2})^2}{(1+\beta^2\chi^{-4})^2}\chi^{-3} = 0. \tag{21}$$

Using the analytical expression of Eq. (20), variations in Q^{-1} with χ for beams with thicknesses of 5, 10, and 20 μm are calculated and depicted in Fig. 1(a). The required parameters for plotting Fig. 1(a) are summarized in Table I, based on which ε and β are calculated as 7.2×10^{-8} $\mathrm{m}^{0.5}$ and 9.33×10^{6} m^{-1}, respectively. Here, the assumed coefficient for the support loss is[26,27] κ=2.1. As depicted in Fig. 1(b), including Q_{TED} in Eq. (20) only slightly changes the value of minimum Q^{-1} and the location of the optimum χ. The same observation can be made in Fig. 2, which shows the optimum calculated length L_{opt} versus the cantilever thickness. In general, as seen in Fig. 1(a), the Q-factor is limited by the support loss for smaller χ and by the air damping for larger χ. Equation (20) indicates, as shown in Fig. 1(a), that increasing the cantilever thickness will monotonically increase the Q-factor; but since in this model the effect of other damping mechanisms is ignored, e.g., especially air friction on the sidewalls, increasing the thickness beyond a limit can result in lower Q-factors.

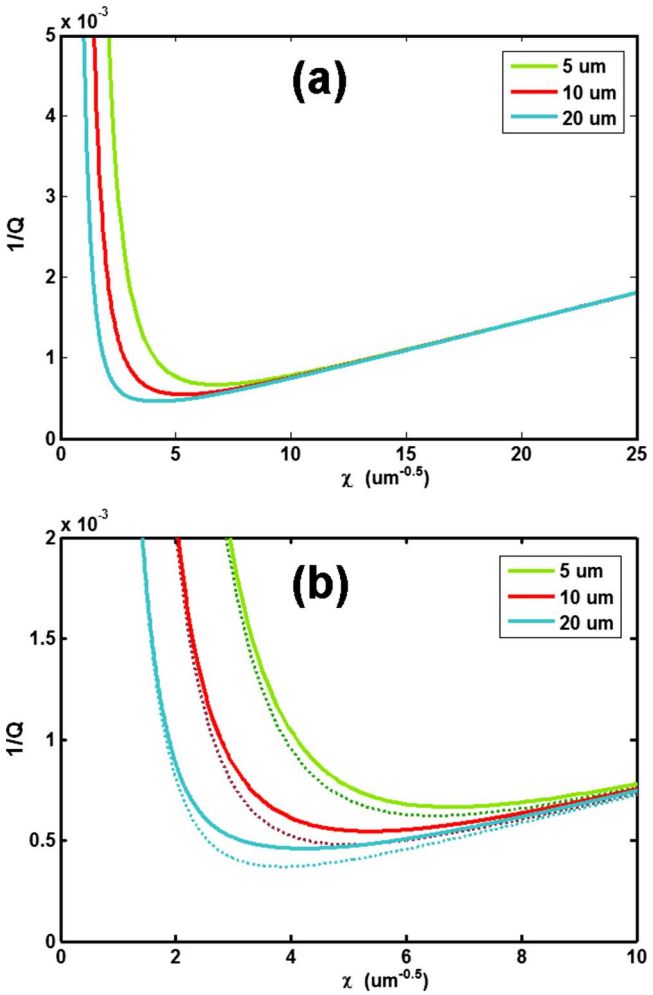

FIG. 1. (Color online) (a) Plots of Q^{-1} vs $\chi=L/H^{1.5}$ for cantilevers with thicknesses of 5, 10, and 20 μm calculated from Eq. (20). (b) Close up of the region of maximum Q comparing the model described by Eq. (20) (solid lines) with the model described by Eq. (15) that excludes TED (dotted lines).

III. EXPERIMENT

Rectangular silicon cantilever beams with lengths and widths ranging from 70 to 1050 μm and from 80 to 230 μm, respectively, have been tested (see Fig. 3). The cantilevers were fabricated using epitaxial silicon wafers with an n-type device layer and a p-type handle layer. The device layer thickness ultimately defined the cantilever thickness. The handle layer was about 525 μm thick. The beams were released by a combination of back-side anisotropic wet etching, using an electrochemical etch-stop technique, and front-side dry etching to define the lateral geometries along the [110] directions. Depending on the thickness of the device layer, the fabricated cantilevers had final silicon thicknesses of 5, 7, 8, 11, and 17 μm, covered with an approximately 0.8 μm thick plasma-enhanced chemical-vapor deposition silicon dioxide layer. It must be pointed out that due to variations in the thickness of the handle wafers, the clamped edge of the cantilevers was not exactly coinciding with the edge of the back-side etched cavity; instead, the cantilevers were supported by a silicon rim of the same thickness, 5–20 μm long for different wafers (see Fig. 3).

Flexural cantilever vibrations are electromagnetically excited: in the presence of a static magnetic flux B in the cantilever length direction, an excitation force is exerted on the cantilever by passing an alternating current through a metal loop along the perimeter of the cantilever (see Fig. 3). In the measurement setup, the cantilevers were at least 525 μm away from the closest parallel surface. The flexural beam vibrations are sensed on chip by a piezoresistive Wheatstone bridge located near the clamped edge of the beam. To have comparable results, it was imperative to keep the resonance amplitude of cantilever confined within the linear bending region of the beam; to this end, depending on the stiffness of the cantilever, in this work the amplitude of excitation current was in the range of 3–20 mA, and the magnetic flux density was between 0.1 and 0.6 T. The transfer characteristics of the resonant cantilevers were recorded by an Agilent Network Analyzer 4395A. Figure 4 shows an

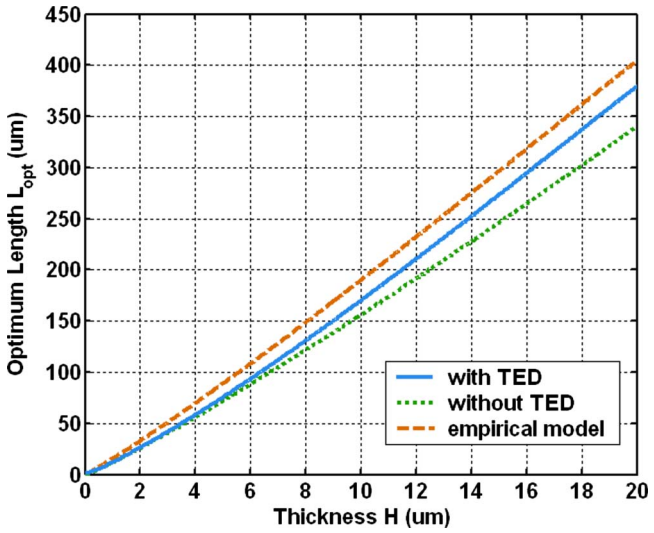

FIG. 2. (Color online) Optimum length of cantilever vs cantilever thickness for achieving maximum Q-factor; the calculation represented by the solid line based on Eq. (21) includes the three dominant damping mechanisms, i.e., the air damping, support loss, and TED, while the calculation of dotted line based on Eq. (16) excludes TED. The dashed line calculation, which also includes the three dominant damping mechanisms, is based on an empirically adjusted model that is described by Eq. (26) with an exponent of support loss $p=2.7$.

amplitude and phase spectrum of a sample device. All measurements were performed at 30 ± 5 °C. For each data point presented in the following section, at least eight transfer characteristics were recorded, and after fitting the data to the

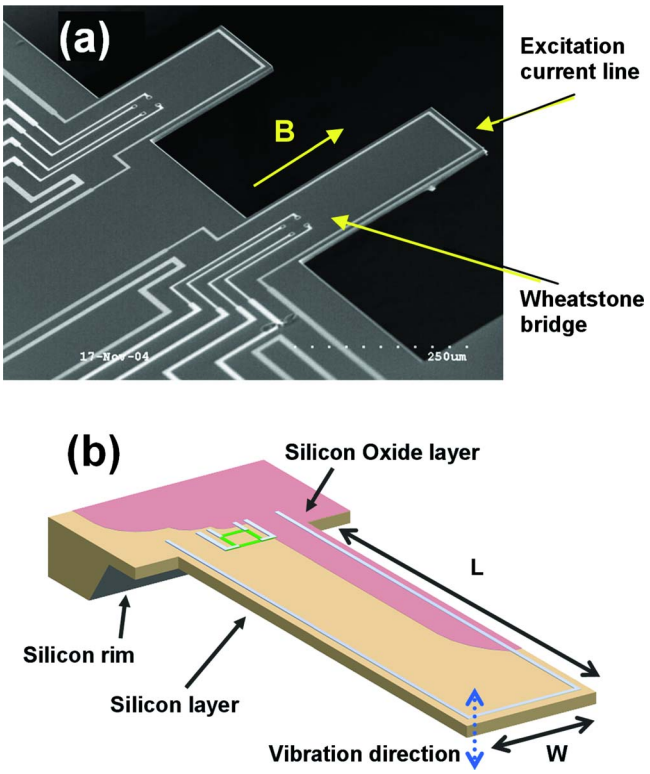

FIG. 3. (Color online) (a) Scanning electron microscopy micrograph of fabricated silicon cantilevers showing the current route along the beam perimeter for excitation of beam vibrations in the presence of a static magnetic flux B; a Wheatstone bridge is located close to the clamped edge to sense the beam deflections. (b) Schematic of a typical cantilever.

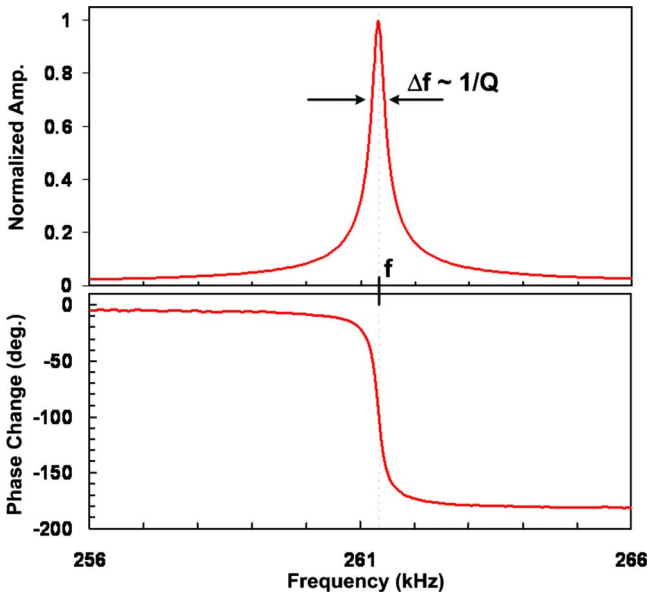

FIG. 4. (Color online) Measured amplitude and phase transfer characteristic of a silicon cantilever beam resonator with L, W, and H of 225, 82, and 11 μm, respectively, around the fundamental flexural resonance frequency.

amplitude transfer characteristic of a second-order system, the extracted resonance frequencies and Q-factors were averaged. For the presented data, the maximum relative standard deviation for the Q-factor is less than 3.3%.

IV. RESULTS AND DISCUSSION

In this section, first the measurement results for different cantilevers are presented and compared with the previously presented analytical predictions. Next, using correction factors, Eq. (20) is adjusted to have the best agreement with the measurement results.

The dependence of the Q-factor on the cantilever length is shown in Fig. 5. In this plot, the width and thickness of the measured cantilevers are 130 and 11 μm, respectively. Two distinct regions can be recognized: in the first region, for a cantilever length smaller than 200 μm, the Q-factor increases with increasing length, whereas in the second region ($L>200$ μm), the Q-factor decreases with an increase in

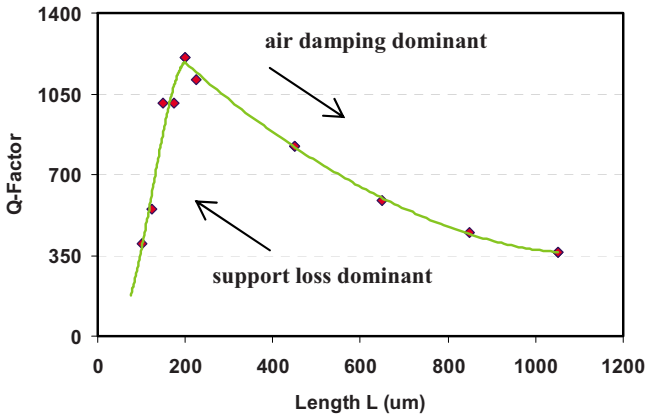

FIG. 5. (Color online) Q-factor as a function of length for cantilevers with width and thickness of 130 and 11 μm, respectively. The solid line is a guide to the eyes only.

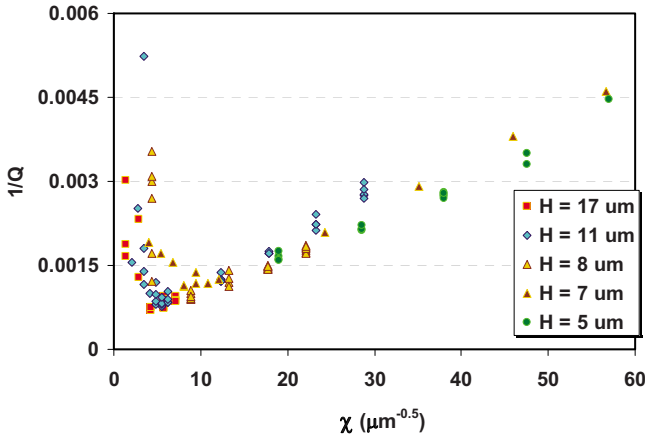

FIG. 6. (Color online) Plot of measured Q^{-1} vs $\chi=L/H^{1.5}$ for cantilevers with thicknesses of 5, 7, 8, 11, and 17 μm. Although not marked in the graph, the widths of the measured cantilevers are not necessarily equal.

length. From Eq. (20) it is known that the dominant damping mechanisms are the air damping and support loss; hence, the two regions in Fig. 5 can be each attributed to one of these damping mechanisms. In the first region, where the length is smaller than 200 μm, i.e., χ is smaller than 5 $\mu m^{-0.5}$, damping is dominated by the support loss. In the second region, for χ larger than 7 $\mu m^{-0.5}$, the air damping is dominant.

To investigate the dependence of the Q-factor on χ, data from all measured cantilevers with different W, L, and H are gathered in Fig. 6, where Q^{-1} is plotted versus χ. It is observed that the Q-factors of beams with different dimensions not only follow similar trends but also overlap for larger χ values. This behavior has been predicted by Eq. (20), as shown in Fig. 1. Equation (20) indicates that for larger χ, where the air damping is the dominant loss mechanism, Q^{-1} increases linearly with χ following a slope given by the coefficient of air damping ε. Therefore, an empirical value for ε can be obtained by a linear regression for all data with $\chi > 12$ $\mu m^{-0.5}$, yielding $\varepsilon_{ipm}=8.2\times10^{-5}$ $\mu m^{0.5}$ [see Fig. 7(a)]. Since the calculated air damping factor from Eq. (12) is 7.2×10^{-8} $m^{0.5}$ (i.e., $\varepsilon=7.2\times10^{-5}$ $\mu m^{0.5}$) for the conditions given in Table I, a correction factor of $c_1=1.14$ can be introduced in Eq. (13) to describe the measured results,

$$Q_{\text{air}}^{-1}=c_1\varepsilon\chi=1.14\times\frac{3}{2}\frac{\pi}{\lambda_n}\left(\frac{3\rho_a^2\eta^2}{\rho_b^3E}\right)^{1/4}\chi. \tag{22}$$

Generally, the energy loss in the region dominated by the air damping is larger than what is predicted by Eq. (10), i.e., by approximating the beam as a string of spheres. A potential explanation for this observation can be attributed to the influence of the beam thickness on the energy loss as the result of, for example, air friction on the beam sidewalls. This explanation is supported by the fact that the measured slope ε for equally thick cantilevers slightly increases by increasing the thickness [see Fig. 7(a)]. In fact, based on the measured data for the air damping dominated region, i.e., χ larger than 12 $\mu m^{-0.5}$, it is found that all the Q^{-1} data points, regardless of the cantilever thickness, will follow almost the identical slopes if they are plotted versus $L/H^{1.25}$, i.e., $H^{0.25}$ χ [see Fig. 7(b)]. In this case, the air damping coefficient, extracted

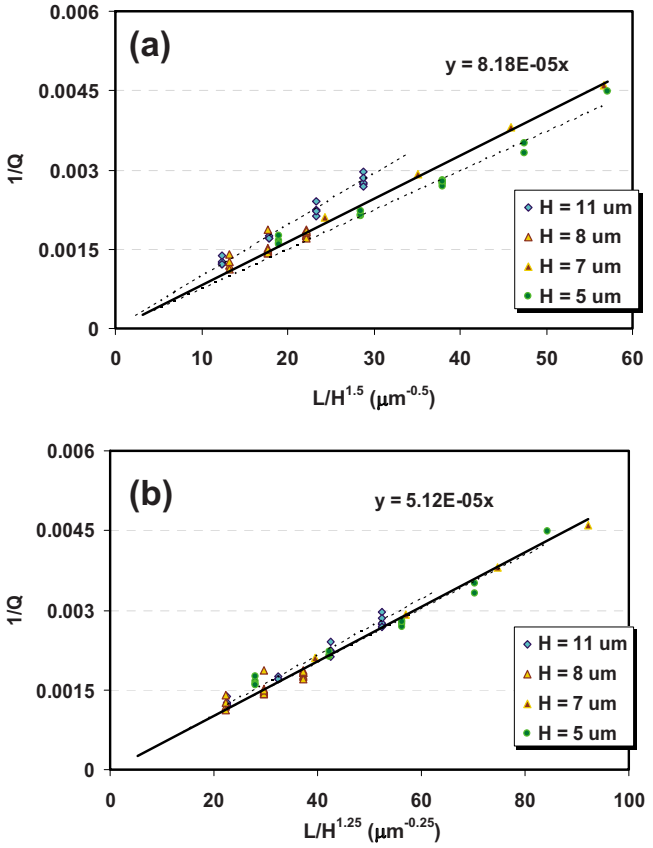

FIG. 7. (Color online) Inverse of Q-factor Q^{-1} as a function of cantilever length L and thickness H: (a) $L/H^{1.5}$ and (b) $L/H^{1.25}$. The exhibited Q-factors belong to cantilever resonators enduring the air damping as the dominant loss mechanism.

from the slope of experimental data, is about 1.6×10^{-6} $m^{0.25}$ (i.e., 5.1×10^{-5} $\mu m^{0.25}$),

$$Q_{\text{air}}^{-1}=1.6\times10^{-6}H^{0.25}\chi. \tag{23}$$

It must be noted that this coefficient is extracted from the data of the fundamental flexural resonance of silicon cantilevers in air and at a temperature of 30 ± 5 °C.

For $\chi<15$ $\mu m^{-0.5}$ (see Fig. 6), unlike in the air damping dominated region, Q^{-1} sharply depends on the device thickness and width. While the thickness dependence is theoretically predicted (as depicted in Fig. 1), the dependence of the Q-factor on W is left unexplained by the basic theory discussed earlier. The width dependence of the Q-factor is further investigated in Fig. 8, which compares the measured Q-factors versus the width of cantilevers with $H=11$ μm and shows that for longer cantilevers (i.e., larger χ values) the Q-factor becomes almost independent of the width; however, when L is smaller (e.g., shorter than 250 μm) the wider beams have noticeably smaller Q-factors. The variation in the Q-factor with W is also shown in Fig. 9 for cantilevers with a fixed length of 400 μm but different thicknesses of 5, 8, and 17 μm. In this figure, the Q-factor variation with width is only observed for cantilevers with χ smaller than 15 $\mu m^{-0.5}$, i.e., for 17 μm thick cantilevers.

Revisiting the theoretical derivations for the air damping expression in Eq. (10), the associated energy loss has become independent of W when the requirement described by

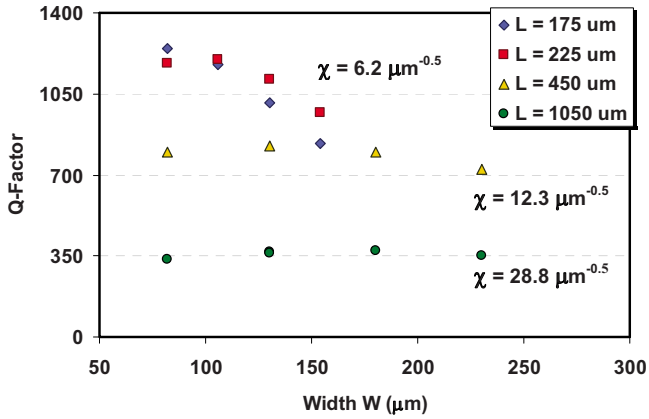

FIG. 8. (Color online) Q-factor as a function of the cantilever width for different lengths; the cantilever thickness is 11 μm.

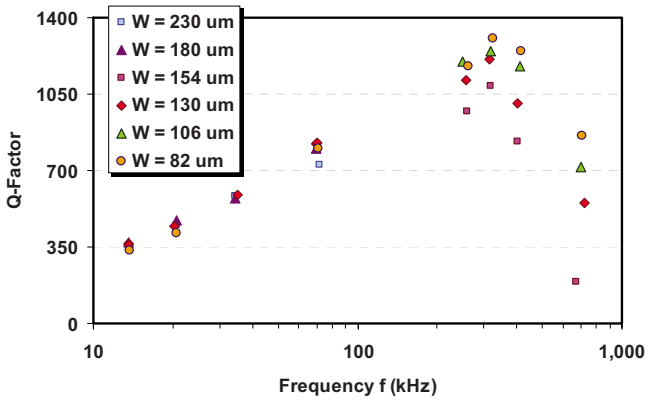

FIG. 10. (Color online) Q-factor as a function of the fundamental flexural resonance frequency for 11 μm thick cantilevers with different widths ranging from 82 to 230 μm.

Eq. (8) is fulfilled. To examine the validity of this simplification, Fig. 10 shows the Q-factors of 11 μm thick cantilevers as a function of their fundamental resonance frequency. Noting that from Eq. (9) the resonance frequency is independent of the cantilever width, as observed in Fig. 10, the width dependence is more pronounced for the Q-factors of cantilevers with higher resonance frequencies. However, cantilevers with higher resonance frequency even better satisfy the condition of Eq. (8); hence, the simplification made in deriving Eq. (16) is valid, and the width variations must be due to another loss mechanism. By comparing the results of Figs. 8–10 and considering the observation that the width dependence is more noticeable in the support loss dominated region, i.e., for smaller lengths, we conclude that using the Q_{clamp} expression of Eq. (14) does not give accurate results for smaller L/H ratios; in fact, Q_{clamp} increases by decreasing the width. Although this observation has been predicted by other theoretical models,[42] the 2D support loss model of Eq. (14) still provides the best overall approximation for our measurement data. Also, since the maximum Q-factor for different cantilever widths occurs at almost identical χ values, as shown in Fig. 6, Eq. (14) can still be helpful in determining the optimum cantilever geometry, despite its shortcoming in including the effect of width. On the other hand, since the fabricated cantilevers are not ideal beams, which must be clamped on a straight semi-infinite sidewall

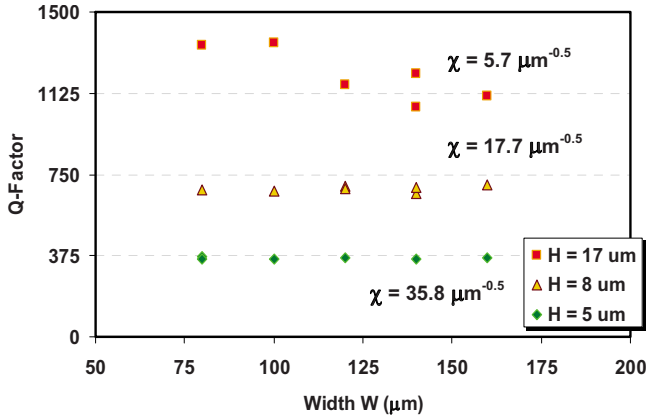

FIG. 9. (Color online) Q-factor as a function of width W for cantilevers with a fixed length $L=400$ μm but different thicknesses of 5, 8, and 17 μm.

as assumed in the derivation of Eq. (14), Q_{clamp} may not be exactly proportional to $(L/H)^3$ but to an L/H ratio with a different exponent.[20] This statement becomes more viable when considering the effect of the silicon rim between the clamped end of the cantilever and the supporting sidewall. To account for this effect, Q_{clamp} can be expressed in a more general form of

$$Q_{\text{clamp}} = \kappa H^{p/2} \chi^{p}. \tag{24}$$

For ideal boundary conditions, i.e., perfect support, the exponent p is 3, while by increasing the length of support rim, a smaller p can give a more accurate expression. By replacing the air damping and support loss terms in Eq. (20) with Eqs. (22) and (24), the Q-factor of resonating cantilevers is obtained as

$$Q^{-1} = 1.14 \times \frac{3}{2}\frac{\pi}{\lambda_n}\left(\frac{3\rho_a^2\eta^2}{\rho_b^3 E}\right)^{1/4}\chi + \kappa^{-1}H^{-p/2}\chi^{-p} + \frac{E\alpha^2 T_o}{\rho_b C_p}\frac{\beta\chi^{-2}}{1+(\beta\chi^{-2})^2}. \tag{25}$$

On the other hand, using the empirically adjusted expression for air damping from Eq. (23), a better agreement with the measurement results of resonant silicon cantilever at a temperature of 30 ± 5 °C can be obtained,

$$Q^{-1} = 1.6 \times 10^{-6} H^{0.25}\chi + \kappa^{-1}H^{-p/2}\chi^{-p} + \frac{E\alpha^2 T_o}{\rho_b C_p}\frac{\beta\chi^{-2}}{1+(\beta\chi^{-2})^2}. \tag{26}$$

The effect of the support loss exponent p is further investigated in Fig. 11, where the Q-factors of cantilevers with thickness and width of 11 and 130 μm, respectively, are compared with the empirical model of Eq. (26). In this figure the measured cantilevers have a silicon rim, approximately 8 μm long. As observed in Fig. 11, a support loss exponent of $p=2.7$ provides the best estimate for the Q-factor of the cantilevers in the support loss dominated region, i.e., $L < 400$ μm. When evaluating the quality of the empirical model of Eq. (26), it must be noted that the calculated maximum Q-factor is expected to be larger than the measured data because Eq. (26) neglects possible additional damping

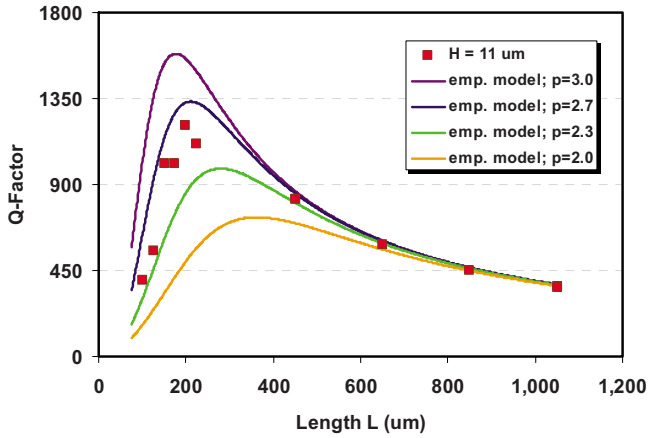

FIG. 11. (Color online) Comparison of measured and calculated Q-factor data for different support loss exponents p; the cantilever thickness and width are 11 and 130 μm, respectively. The Q-factor calculation is based on the empirical model described by Eq. (26).

mechanisms, e.g., the volume loss and the air friction, as well as the effect of ambient conditions, e.g., temperature. Moreover, the influence of the silicon oxide layer covering the cantilever ($\sim$0.8 μm) and also the effect of small variations in the thickness of fabricated beams are not considered in the calculation. Finally, the influence of the cantilever width is also not included in Eq. (26). It should be emphasized that unlike the absolute value of the calculated Q-factor, the optimum calculated length L_{opt} does not vary significantly with the empirical and theoretical values of p =2.7 and 3 (where L_{opt}=210 and 176 μm, respectively).

A comparison of different models for describing the Q-factor versus the resonance frequency f is presented in Figs. 12 and 13. Figure 12 summarizes the Q-factor data for 140 μm wide cantilevers with thicknesses of 5, 8, and 17 μm and compares them to the calculated data based on the combined effects of support loss using Eq. (24) with p =2.7, TED using Eq. (18), and three different air damping models: (A) the corrected analytical air damping model described by Eq. (25), (B) the well-known analytical air damping model proposed by Sader,[30] and (C) the empirical model of air damping according to Eq. (26). Overall, model C based on Eq. (26) best describes the experimental data [see Fig. 12(c)]. This observation becomes even more evident in Fig. 13, where the results obtained from the three models are compared closely together and to the measurement data of cantilevers with width and thickness of 130 and 11 μm, respectively. For lower resonance frequencies (i.e., longer cantilevers), model C perfectly matches the measurement data, while the two other models closely follow the data trend. However, for higher frequency (i.e., shorter cantilevers), there is a frequency gap between the measurement and calculations. Since in Fig. 11 the result of model C has exhibited an acceptable match with the experimental data for the shorter cantilevers, the presence of the frequency gap in Fig. 13 is believed to be associated with the discrepancy between the calculated and measured frequencies in the shorter cantilevers. An explanation for this effect is referred to the increasing significance of nonideal boundary conditions (e.g., the presence of silicon rim and nonideal clamped edge) for shorter beams.

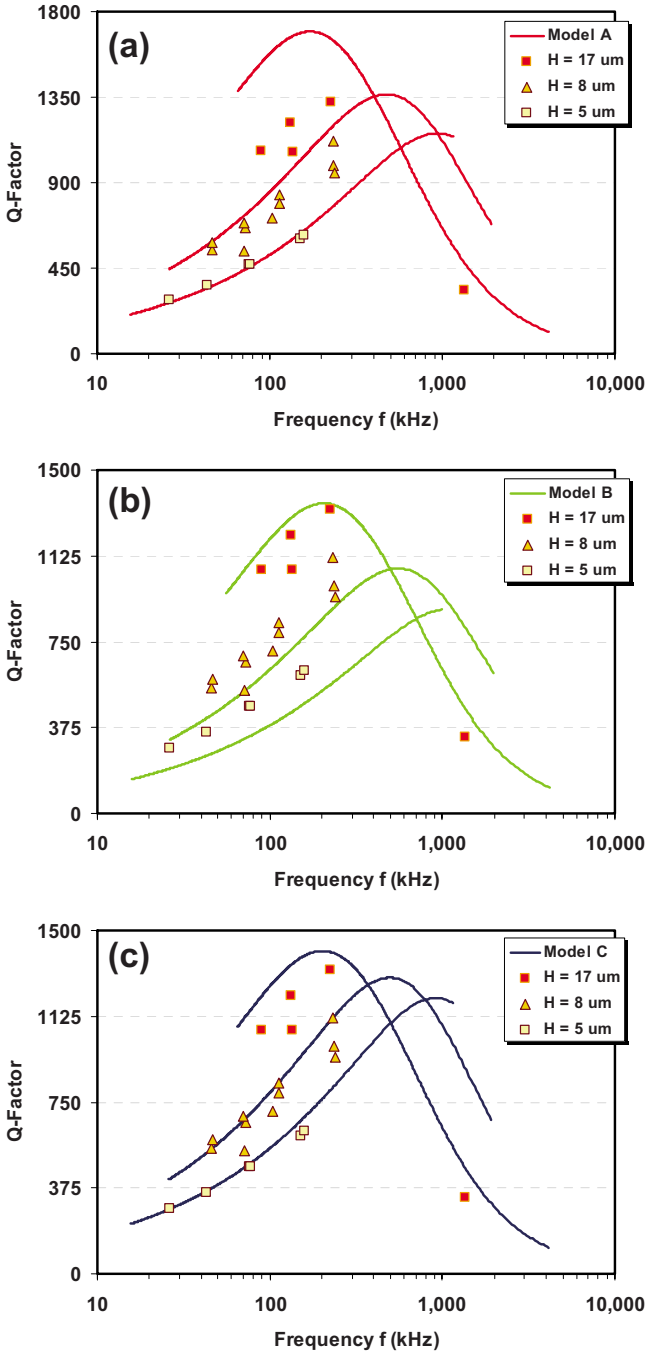

FIG. 12. (Color online) Q-factor as a function of resonance frequency for 140 μm wide cantilevers. The measured data are compared with the following models: (a) model A, the proposed analytical model of Eq. (25), (b) model B, in which the air damping is described by Sader's analytical model (Ref. 30), and (c) model C, the proposed empirical model of Eq. (26). The x-axis indicates the corresponding fundamental flexural resonance frequency.

The presence of resonant modes in close frequency proximity (coupled peaks) is another factor that can undermine the analytical predictions. It is well known that the presence of multiple peaks in close vicinity results in reduction in the Q-factor.[24] This effect can be observed in Fig. 14, which demonstrates two examples of significant aberration of the measured Q-factors from the analytical prediction for cantilevers with lengths of 100 and 150 μm. In this figure, the cantilevers width and thickness are 11 and 82 μm, respec-

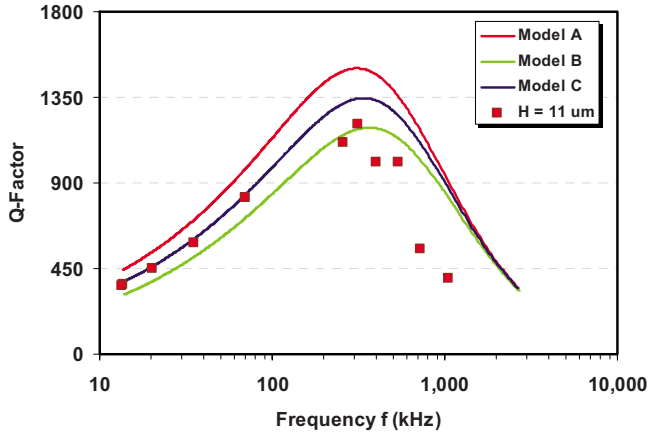

FIG. 13. (Color online) Q-factor as a function of resonance frequency for cantilevers with thickness and width of 11 and 130 μm, respectively. The measured data are compared with the results of previously mentioned models A, B, and C. The x-axis indicates the corresponding fundamental flexural resonance frequency.

tively. The analytical calculation is based on Eq. (26) with a support loss exponent $p=2.75$. In all presented plots in this work, the data points associated with coupled peaks are omitted unless they are explicitly marked.

Finally, the optimal cantilever geometry for achieving the maximum Q-factor given by Eq. (21) can be revised by including the fit parameter as in Eqs. (25) or (26). Similar to Eq. (21), the optimal χ can be calculated by finding the minimum Q^{-1} in Eq. (26). Based on this calculation, for $p=2.7$, the optimal length, as a function of thickness, is presented with a dashed line in Fig. 2. The required parameters for plotting Fig. 2 are summarized in Table I. It is observed that using the empirically adjusted model only slightly affects the predicted optimal cantilever length for a given thickness; therefore, Fig. 2 can be used as a simple look-up graph to find the cantilever dimension for maximizing the Q-factor of the fundamental flexural resonance mode.

V. CONCLUSION

Combining analytical derivations and experimental results, two models are developed to estimate the optimum dimensions of resonant rectangular cantilever beams for achieving maximum quality factor in air at the fundamental resonance. For silicon cantilevers with thicknesses between 5 and 17 μm, it has been calculated that the reciprocal of Q-factor is linearly proportional to $L/H^{1.5}$ if this ratio is larger than 15 $\mu m^{0.5}$. This behavior indicates that the air damping is the dominant loss mechanism for cantilevers with such length to thickness ratios; however, a close examination of the measured quality factors of these cantilevers shows that they exhibit almost identical quality factors if they share the same ratio of $L/H^{1.25}$, or in other words, the air damping seems to be proportional to $L/H^{1.25}$. Also, it has been shown that the effect of cantilever width may be neglected in analytical calculations, and the measurement results of cantilevers with large $L/H^{1.5}$ confirm this assumption. In contrast, with the support loss being a significant contributor to the damping, in short cantilevers (i.e., $L/H^{1.5}<15$ $\mu m^{0.5}$) the Q-factor becomes a strong function of the cantilever width. Nevertheless, it is observed that the maximum measured Q-factor of cantilevers with different widths but same thickness occurs almost at the same length. Moreover, it is recognized that the support loss equation must be adjusted to include the effect of imperfectness on the cantilever support (i.e., the clamped edge) when compared to the ideal boundary condition. Combining the corrected equations of air damping and support loss with the well-known Zener approximation for TED has enabled us to calculate the optimum lengths of resonant cantilevers with given thicknesses to achieve the maximum possible quality factor for the fundamental flexural resonance mode in air.

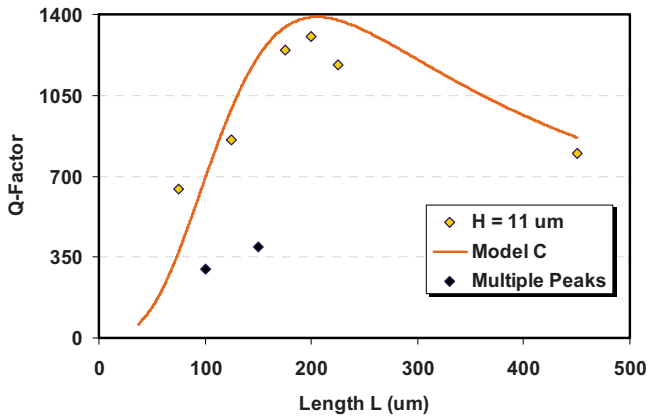

FIG. 14. (Color online) Reduced Q-factors for two cases of cantilevers with lengths of 100 and 150 μm (dark diamonds) due to occurrence of multiple peaks in a close frequency proximity (coupled peaks); the thickness and width of the cantilevers in this graph are 11 and 82 μm, respectively. The solid line shows the Q-factor calculation based on Eq. (26).

ACKNOWLEDGMENTS

The authors would like to thank A. Shah, S. Sutcu, A. Brown, and S. Mohammadi for their valuable help with the device characterization. This work has been funded in part by the National Science Foundation under Grant No. 0304009.

[1] T. Thundat, E. A. Wachter, S. L. Sharp, and R. J. Warmack, Appl. Phys. Lett. **66**, 1695 (1995).
[2] A. Boisen, J. Thaysen, H. Jensenius, and O. Hansen, Ultramicroscopy **82**, 11 (2000).
[3] D. Lange, C. Hagleitner, A. Hierlemann, O. Brand, and H. Baltes, Anal. Chem. **74**, 3084 (2002).
[4] N. V. Lavrik, M. J. Sepaniak, and P. G. Datskos, Rev. Sci. Instrum. **75**, 2229 (2004).
[5] Y. Xu, J. T. Lin, B. W. Alphenaar, and R. S. Keynton, Appl. Phys. Lett. **88**, 143513 (2006).
[6] W. H. King, Anal. Chem. **36**, 1735 (1964).
[7] J. P. Cleveland, S. Manne, D. Bocek, and P. K. Hansma, Rev. Sci. Instrum. **64**, 403 (1993).
[8] M. Li, H. X. Tang, and M. L. Roukes, Nat. Nanotechnol. **2**, 114 (2007).
[9] J. R. Vig and F. L. Walls, in Proceedings of the 2000 IEEE/EIA International Frequency Control Symposium and Exhibition, Kansas City, MO, 2000, p. 30-3.
[10] L. Rodriguez-Pardo, J. F. Rodriguez, C. Gabrielli, and R. Brendel, IEEE Sens. J. **5**, 1251 (2005).
[11] A. N. Cleland and M. L. Roukes, J. Appl. Phys. **92**, 2758 (2002).
[12] M. B. Viani, T. E. Schaffer, A. Chand, M. Rief, H. E. Gaub, and P. K. Hansma, J. Appl. Phys. **86**, 2258 (1999).
[13] J. A. Sidles and D. Rugar, Phys. Rev. Lett. **70**, 3506 (1993).
[14] W. Jing, J. E. Butler, D. S. Y. Hsu, and T. C. Nguyen, in Technical Digest. MEMS 2002 IEEE International Conference, Las Vegas, NV, 2002, p. 657-60.

[15]F. R. Blom, S. Bouwstra, M. Elwenspoek, and J. H. J. Fluitman, J. Vac. Sci. Technol. B **10**, 19 (1992).
[16]J. W. M. Chon, P. Mulvaney, and J. E. Sader, J. Appl. Phys. **87**, 3978 (2000).
[17]W. E. Baker, W. E. Woolam, and D. Young, Int. J. Mech. Sci. **9**, 743 (1967).
[18]S. A. L. Glegg, J. Sound Vib. **87**, 637 (1983).
[19]G. R. Torr, Am. J. Phys. **52**, 402 (1984).
[20]M. C. Cross and R. Lifshitz, Phys. Rev. B **64**, 085324 (2001).
[21]C. Zener, Phys. Rev. **53**, 90 (1938).
[22]R. Lifshitz and M. L. Roukes, Phys. Rev. B **61**, 5600 (2000).
[23]S. Reid, G. Cagnoli, D. R. M. Crooks, J. Hough, P. Murray, S. Rowan, M. M. Fejer, R. Route, and S. Zappe, Phys. Lett. A **351**, 205 (2006).
[24]V. B. Braginsky, *Systems with Small Dissipation* (University of Chicago Press, Chicago, 1985).
[25]J. Yang, T. Ono, and M. Esashi, J. Microelectromech. Syst. **11**, 775 (2002).
[26]K. Y. Yasumura, T. D. Stowe, E. M. Chow, T. Pfafman, T. W. Kenny, B. C. Stipe, and D. Rugar, J. Microelectromech. Syst. **9**, 117 (2000).
[27]Z. L. Hao, A. Erbil, and F. Ayazi, Sens. Actuators, A **109**, 156 (2003).
[28]W. E. Newell, Science **161**, 1320 (1968).
[29]K. Kokubun, M. Hirata, H. Murakami, Y. Toda, and M. Ono, Vacuum **34**, 731 (1984).
[30]J. E. Sader, J. Appl. Phys. **84**, 64 (1998).
[31]L. D. Landau and E. M. Lifshitz, *Fluid Mechanics*, 2nd ed. (Elsevier, New York, 2004).
[32]K. Yum, Z. Wang, A. P. Suryavanshi, and M.-F. Yu, J. Appl. Phys. **96**, 3933 (2004).
[33]K. Kokubun, M. Hirata, M. Ono, H. Murakami, and Y. Toda, J. Vac. Sci. Technol. A **5**, 2450 (1987).
[34]G. Y. Chen, R. J. Warmack, T. Thundat, D. P. Allison, and A. Huang, Rev. Sci. Instrum. **65**, 2532 (1994).
[35]H. Hosaka, K. Itao, and S. Kuroda, Sens. Actuators, A **49**, 87 (1995).
[36]D. A. Walters, J. P. Cleveland, N. H. Thomson, P. K. Hansma, M. A. Wendman, G. Gurley, and V. Elings, Rev. Sci. Instrum. **67**, 3583 (1996).
[37]P. I. Oden, G. Y. Chen, R. A. Steele, R. J. Warmack, and T. Thundat, Appl. Phys. Lett. **68**, 3814 (1996).
[38]D. W. Stauff and D. J. Montgomery, J. Appl. Phys. **26**, 540 (1955).
[39]S. Kirstein, M. Mertesdorf, and M. Schonhoff, J. Appl. Phys. **84**, 1782 (1998).
[40]T. Ikehara, J. Lu, M. Konno, R. Maeda, and T. Mihara, J. Micromech. Microeng. **17**, 2491 (2007).
[41]L. Rosenhead, *Laminar Boundary Layers: An Account of the Development, Structure, and Stability of Laminar Boundary Layers in Incompressible Fluids, Together with a Description of the Associated Experimental Techniques* (Clarendon, Oxford, 1963).
[42]D. M. Photiadis and J. A. Judge, Appl. Phys. Lett. **85**, 482 (2004).
[43]A. Duwel, R. N. Candler, T. W. Kenny, and M. Varghese, J. Microelectromech. Syst. **15**, 1437 (2006).
[44]K. Naeli, P. Tandon, and O. Brand, in Solid-State Sensors, Actuators and Microsystems Conference, Lyon, France, 2007, pp. 245–248.
[45]S. Timoshenko, D. H. Young, and W. Weaver, *Vibration Problems in Engineering*, 4th ed. (Wiley, New York, 1974).
[46]A. Nathan and H. Baltes, *Microtransducer CAD: Physical and Computational Aspects* (Springer, New York, 1999).